Impurities and geometrical effects on the electron energy spectrum of quantum rings

G. A. Farias,[1,*] M. H. Degani,[1,†] J. A. K. Freire,[1,‡] J. Costa e Silva,[1,§] and R. Ferreira[2,‖]
[1]*Departamento de Física, Universidade Federal do Ceará, Caixa Postal 6030, Campus do Pici, Fortaleza, 60455-900 Ceará, Brazil*
[2]*Laboratoire Pierre Aigrain, Ecole Normale Superieure, 24 Rue Lhomond, F75005 Paris, France*
(Received 19 December 2006; revised manuscript received 10 September 2007; published 21 February 2008)

We calculate the energy spectrum of semiconductor quantum rings. We consider a realistic model consisting of rings with finite sizes and barrier potential and take into account an external magnetic field applied perpendicularly to those structures. The solutions of the Schrödinger equations are found using an evolution method not limited to small perturbations. The magnetic field leads to the Aharonov-Bohm (AB) oscillations, which are strongly dependent on the presence of static defects. We consider charged impurities and interface roughness, which break the cylindrical ring symmetry and can strongly affect, or even destroy, the AB oscillations.

DOI: 10.1103/PhysRevB.77.085316 PACS number(s): 73.21.−b, 73.20.Hb

I. INTRODUCTION

Recent progress in nanofabrication techniques has allowed the construction of a new confined structure called a quantum ring (QR). The QR is often modeled by a cylindrical quantum dot with an internal axially symmetric cavity. This unique geometry has attracted much attention in the last few years.[1–10] In the presence of an axially directed magnetic field, persistent current and oscillations of the electron energy as a function of the magnetic flux (Aharonov-Bohm effect) were found to occur.[11] The Aharonov-Bohm (AB) oscillations are due to a change of phase on the wave function when the magnetic flux ϕ passing through the ring reaches the magnetic quantum flux $\phi_0=h/e$ (h is the Planck constant and e is the electronic charge). The structural modification makes the electronic properties of rings quite different from the dots. Quantum rings can be obtained, for example, from GaAs quantum dots which are partially covered with Ga(Al)As,[3] such that the original dots develop a hole in their center and get a ringlike shape. Other materials, such as InGaN/GaN,[2] In(Ga)As,[8] and InAs/InP,[7] have also been used in the formation of QRs.

The electronic states of QR's in the presence of external fields have been the subject of intense investigation in recent years.[5,6,12–19] Some works pointed out that optical properties and electronic states of actual structures are strongly affected by impurities and geometrical imperfections of the system. Monozon and Schmelcher[6] have considered the case of an impurity center in a semiconductor QR and calculated analytically the binding energy of an electron in the presence of crossed magnetic and electric fields, considering the QR potential as an infinite barrier. Bruno-Alfonso and A. Latgé[12,15] also studied the effects of an impurity on QRs subjected to an external magnetic field. They used a variational approach to obtain the 1s-like shallow-donor impurity states, with the impurity located inside the QR and at a medium distance of the internal and external radii. They observed that, in this particular case, the binding energy is essentially independent of the external magnetic field. Dias da Silva *et al.*[5] analyzed the effects of impurities on the AB oscillations in QRs and their subsequent effects on the photoluminescence emission. Monozon and Schmelcher[6] considered an analytical approach to the problem of an impurity in a QR, but their results are valid only for particular values of the external electrical or magnetic field strengths and for particular geometrical parameters associated with confinement in the QR.

Geometrical changes in QRs also affect the electronic properties. Recently, Lavenère-Wanderley *et al.*[20] and Bruno-Alfonso and Latgé[15] analyzed the effects of eccentricity in QRs, which can suppress the AB oscillations. Gridin *et al.*[21] studied the electronic states in QRs with arbitrary shapes, showing the presence of state localization in regions of maximal curvature (at $B=0$). In all calculations, we observe the same restrictions due to the perturbation method or to the fact that the carriers are confined by infinite barriers outside the ring.

In the present paper, we study the energy spectrum of an electron in semiconductor quantum rings considering an external magnetic field applied perpendicularly to those structures, taking into account a realistic model consisting of rings with finite size and barrier potential. The presence of one or two positive and negative hydrogenic impurities is considered and its effect on the AB oscillations is investigated. The effects on the energy spectrum due to an arbitrary deformation, such as lack of cylindrical symmetry on the geometry of the structure and roughness on the ring surfaces, are also considered. Contrary to previous theoretical studies, we apply a nonperturbative method that can be used for any magnetic field intensity, location of the impurities, and ring shape. Moreover, it allows the study of excited ring states and can also be easily generalized to tackle different radial potential profiles (and in particular, smoother ones in the presence of interdiffusion).

The paper is organized as follows. In Sec. II, we present our model of a QR and discuss the method used to solve the Schrödinger equation. In Sec. III, we present the effects of the presence of impurities close to the ring on its electronic levels. In Sec. IV, we analyze the AB oscillations in rings that present an eccentricity or roughness of surfaces. Finally, in Sec. V, we present our conclusions.

II. HAMILTONIAN MODEL

We consider a QR formed by the revolution around the z axis of a cube with internal (external) in-plane radius $|\vec{\rho}|=a(b)$ and ring height h_z along the growth direction (z) (see

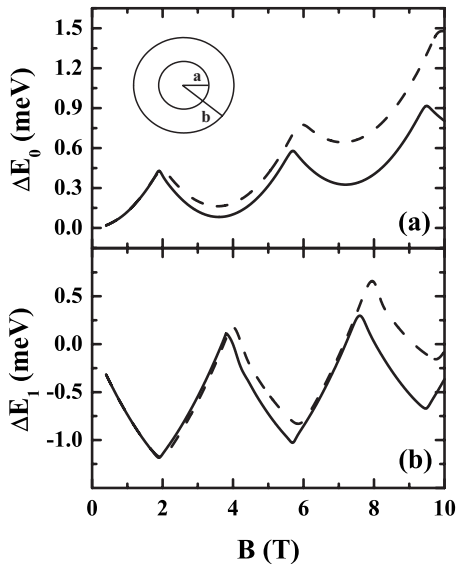

FIG. 1. Energy shift $\Delta E_n = E_n(B) - E_n(B=0)$ as a function of the external magnetic field of the (a) ground state and (b) first excited state, with rings of average size $|\vec{\rho}| = (a+b)/2 = 190$ Å and width $b-a = 60$ Å (solid line) and $b-a = 120$ Å (dashed line), respectively.

inset of Fig. 1). Usually $h_z \ll a, b$ so that one can approximately decouple the electron motions along the z direction and in the x, y plane and retain in the analysis only the first state along the z direction (adiabatic approximation). Consequently, without loss of generality, our system can be considered two dimensional, with the electron confined in the plane $z=0$. We also consider an external uniform magnetic field B parallel to the z axis and hydrogenic impurities located at $\vec{\rho} = \vec{\rho}_{imp}$ and at a distance $z = z_i$ from the QR plane. Within the effective-mass approximation, the confining potential is given by

$$V_e(\vec{\rho}) = \begin{cases} 0 & \text{if } a < |\vec{\rho}| < b \\ V_0 & \text{otherwise.} \end{cases} \tag{1}$$

The QR is embedded in a (GaAl)As matrix with the barrier height $V_0 = 190$ meV, corresponding to an Al concentration of $x = 0.25$. Considering a position independent parabolic conduction band, the Hamiltonian can be written as

$$H = \frac{1}{2m^*}(\vec{p} + e\vec{A})^2 + V_e(\vec{\rho}) + \sum_{i=1}^{N} V_{imp}^i + \delta V_e(\vec{\rho}), \tag{2}$$

where m^* is the electron effective mass ($m^* = 0.067 m_0$ with m_0 as the free electron mass) and the vector potential is chosen in the symmetric gauge $\vec{A} = \frac{1}{2}\vec{B} \times \vec{\rho}$. The potential due to each impurity is taken of the form $V_{imp}^i = \frac{Z_i e}{4\pi\epsilon\epsilon_0} / [(\vec{\rho} - \vec{\rho}_{imp})^2 + z_i^2]^{1/2}$, with Z_i as the impurity charge, N is the number of impurities, and the dielectric constant of the GaAs is taken as $\epsilon = 12.5$. This form follows after averaging the three-dimensional Coulomb potential by the z-related electron density, which is assumed to be strongly localized inside the ring (δ-like along z). The last term in Eq. (2) is a perturbation to the confining potential that breaks the cylindrical symmetry. We shall consider in Sec. IV both a geometrical (eccentricity of QR shape) and interface-related disorder (interface roughness) case.

The evolution method used to obtain the energy levels is based on the solution of the time-dependent Schrödinger equation.[22–24] It is not limited to small perturbations and can be used for nonlinear effects, including extreme conditions created by laser pulses. Using this method, only states of interest are involved and the calculation can be made to scale linearly with the size of the system, contrary to methods based on the linear response formalism which involve diagonalization of large matrices. Another advantage of this method is that it does not use a basis expansion or adjustable parameters and the effect of external fields is treated in a nonperturbative way. These features are very important to treat the impurity problem. In fact, due to the lack of symmetry, it is often very difficult to choose a reasonable trial wave function (variational approach) or ensemble of wave functions (method of expansion onto a basis) to describe the electronic states for any magnetic field intensity. Indeed, in the low magnetic field regime, the Coulomb field effect is more important than the magnetic field effect, while for high magnetic fields, the opposite situation occurs.

Let us briefly recall the main aspects of the evolution method (for more detail, see Refs. 22 and 23). In order to solve the time-dependent Schrödinger equation in general, it is not possible to perform the exponentiation of an operator exactly, and one must bring the operators to a diagonal form. The time evolution of the wave function after one-time step Δt is given by

$$\Psi(\vec{r}, t + \Delta t) = e^{-iH\Delta t/\hbar}\Psi(\vec{r}, t). \tag{3}$$

Since the time evolution operator is unitary, the normalization of the wave function is preserved and thus guarantees the conservation of the probability and the unconditional stability of the method. For a time-independent Hamiltonian, the propagation is time-reversal invariant and conserves the total energy. The evolution method has been applied to obtain an arbitrary number of eigenstates in various semiconductor structures at $B=0$.[22–24] Here, we generalize this approach to tackle the magnetic field effects. We show in the Appendix how to numerically implement this method. Basically, in order to obtain the electron eigenstates, we start from an initial Gaussian wave packet and perform (according to the outline described in the Appendix) its evolution in the imaginary time domain, that is, one substitutes t by $-i\tau$. After a few steps, the wave function converges to the ground state of the system. The excited states are obtained using the same procedure, in combination with a Gram-Schmidt orthonormalization.

In order to illustrate the evolution method for the QRs, we show in Fig. 1 the shifts $\Delta E_n = E_n(B) - E_n(B=0)$ in the energies of the ground ($n=0$) and the first excited ($n=1$) states as a function of the external magnetic field, with different values of ring size for ideal QRs (without the presence of impurities). As can be seen, the AB oscillations are present and the period of oscillations slightly increases with the energy level and ring width. This fact was expected both because the excited state is more spread inside the ring region than the

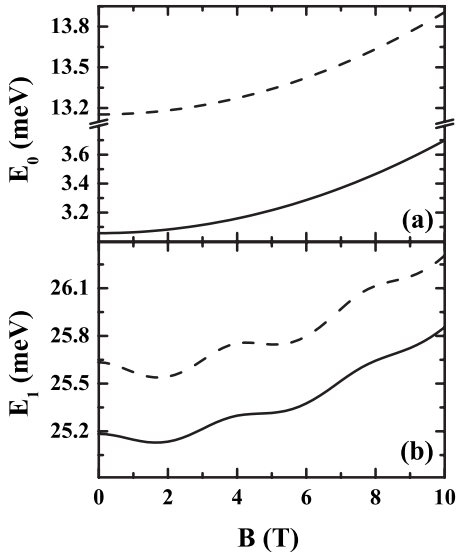

FIG. 2. Energy of the (a) ground state and (b) first excited state as a function of the external magnetic field for a positive hydrogenic impurity at two different distances z_i to the ring plane $z_1 = 10$ Å (solid line) and $z_1 = 30$ Å (dashed line), with $a = 140$ Å and $b = 240$ Å.

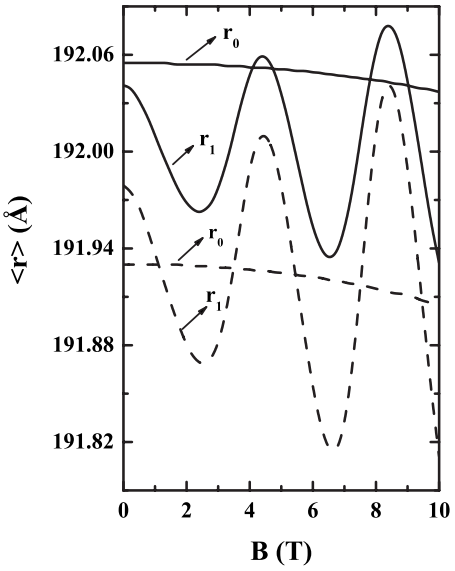

FIG. 3. Average in-plane radius of the ground (r_0) and first excited (r_1) states as a function of the external magnetic field for the same parameters as in Fig. 2.

ground state and because the ring area increases with its width. In addition, since the magnetic flux through the ring decreases with both factors, a more intense magnetic field is necessary in order to observe the AB oscillations.

In the following sections, we consider the effects of different perturbations of the ideal QRs, which are expected to be present in actual structures. Our aim is to analyze the robustness of the AB oscillations against static disorder. As we shall see, realistic perturbations strongly affect (or even destroy) the AB oscillations in QRs.

III. EFFECTS OF CHARGED IMPURITIES ON ELECTRONIC LEVELS

To analyze the effects of hydrogenic impurities, we consider initially a ring with size $a = 140$ Å and $b = 240$ Å and one single impurity with positive charge located at the position $\vec{r}_{imp} = (190\ \text{Å}, 0, z_i)$ with two different distances to the ring plane, that is, $z_1 = 10$ Å and $z_2 = 30$ Å, respectively. Figures 2 and 3 present, respectively, the energies and the average in-plane radii of the ground and first excited states as a function of the external magnetic field. As is evident, the effects on the electronic structure due to a single hydrogenic impurity is similar to the one resulting from the presence of an external electric field applied in the ring plane (see, e.g., Ref. 6), representing a break of symmetry related to the field acting on the confined electron. As shown in Fig. 2(a), the AB oscillations were suppressed for the ground state for the two impurity positions z_i. The hydrogenic potential breaks down the cylindrical symmetry and the electron ground state confinement is strongly related to the impurity charge. The reason is that for a positive impurity, the electron tends to be bounded and consequently confined near the impurity charge. As seen in Fig. 3, the average radius for the ground state is very close to the in-plane impurity position of 190 Å and almost independent of the magnetic fields below 10 T. The first excited state [Fig. 2(b)] presents instead small energy oscillations due to its larger delocalization, showing that the external magnetic field now starts to play an important role. The oscillations of the energies with B are accompanied by an analogous effect on the average radius, as shown in Fig. 3. However, the hydrogenic potential is very strong even for the first excited state and one observes oscillations on the average radius smaller than 1 Å. Figures 2 and 3 show that the ground state AB oscillations are completely suppressed by the presence of a "near" impurity. More generally, we have checked that these oscillations start to be destroyed for an impurity distance such that the electrostatic perturbation to the ground state becomes comparable to the characteristic QR energy spacing, i.e., when $e^2/(4\pi\epsilon\epsilon_0|z_i|) \geqslant E_1(0) - E_0(0)$. For the parameters of the QR in Fig. 2, this corresponds to $|z_i| \leqslant 1,\ 5\langle r_0\rangle \approx 1,\ 5(a+b)/2$.

Let us consider the same rings, but now with a negative hydrogenic impurity at the same positions as in Figs. 2 and 3. Figure 4 presents the energies of the ground and first excited states as a function of the external magnetic field. Again, due to the symmetry break, the AB oscillations were suppressed for the ground state energy at two positions of the impurity. The first excited state energy presents small oscillations as long as the impurity stays away from the ring plane. Since the impurity is negative, the energies are very different from the ones with a positive charge. Although the average radius for a positive (Fig. 3) and negative impurity (not shown) is almost of the same order of magnitude, we have nevertheless checked that the electron wave function becomes localized along the circumference of the ring in the presence of an impurity charge: for the negative (positive) impurity charge, the electron is confined inside the ring the farthest from the repulsive center (the nearest from the attractive center). The

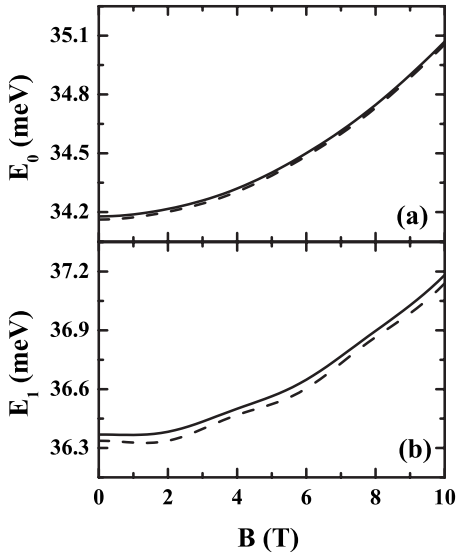

FIG. 4. Energy of the (a) ground state and (b) first excited state as a function of the external magnetic field for a negative hydrogenic impurity at two different distances z_i to the ring plane: $z_1 = 10$ Å (solid line) and $z_2 = 30$ Å (dashed line) for the same QR parameters as in Fig. 2.

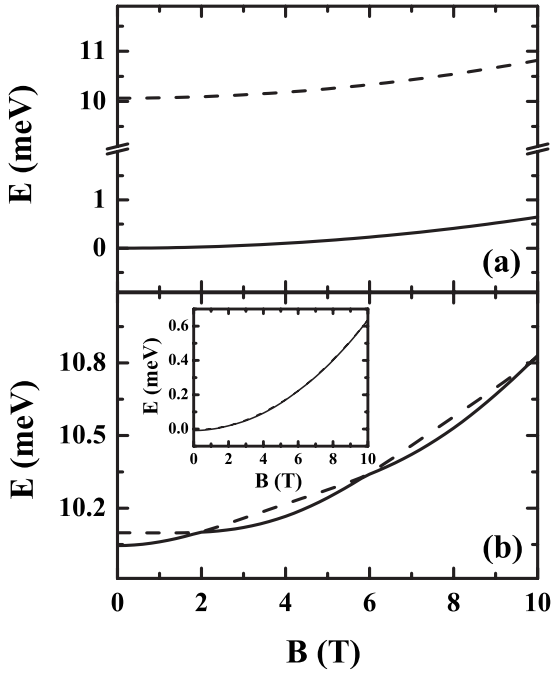

FIG. 5. Energy of the ground state (solid line) and first excited state (dashed line) with two positive hydrogenic impurities nearby a QR with size $a = 140$ Å and $b = 240$ Å, with the first impurity at $\vec{r}_{imp}^{(1)} = (190\ \text{Å}, 0, z_1)$ and the second one at $\vec{r}_{imp}^{(2)} = (-190\ \text{Å}, 0, z_2)$. (a) $z_1 = 10$ Å and $z_2 = 30$ Å and (b) $z_1 = z_2 = 30$ Å ($z_1 = z_2 = 10.0$ Å in the inset).

ground state localization diametrically opposed to the impurity, as well as the suppression of its AB oscillation, starts occurring when the electrostatic drop along the QR diameter becomes larger than the characteristic QR energy spacing $E_1(0) - E_0(0)$ (see also Ref. 6). For large diameter QRs, this rough criterion also leads to $|z_i| \leqslant 1,5\langle r_0 \rangle$.

Now we will consider the effects of two hydrogenic impurities of the same signal in a QR with size $a = 140$ Å and $b = 240$ Å, with the first impurity at $\vec{r}_{imp}^{(1)} = (190\ \text{Å}, 0, z_1)$ and the second one at $\vec{r}_{imp}^{(2)} = (-190\ \text{Å}, 0, z_2)$. The existence of two impurities presents a more complex analysis and the existence or not of AB oscillations depends strongly on the relative positions of impurities along z. Figure 5 presents the energies of the ground and first excited states as a function of the external magnetic field for the two attractive centers. In Fig. 5(a), we observe that the energies of the ground and first excited states do not oscillate if $z_1 \neq z_2$. In this case, we have two nonsymmetric attractive centers, which present in the QR region a nonvanishing average gradient potential (like in the case of one impurity center in Fig. 2). If the hydrogenic impurities are at the same distance of the ring plane ($z_1 = z_2$), the total potential is symmetric (the in-plane average of the gradient potential vanishes for any QR state) and consequently we can see in Fig. 5(b) weak oscillations in both energy levels. The amplitudes of the energy oscillations decrease rapidly when the impurities approach the QR for $z_1 = z_2$ because of the strong perturbation of the impurities close to the ring plane.

Considering two negative hydrogenic impurities, in Fig. 6, we present the energies of the ground and first excited states and the ground state average radius as a function of the external magnetic field. From Fig. 6, we can see that all energy levels oscillate regardless of the positions of the hydrogenic impurities. This means that with two negative hydrogenic impurities, the magnetic field is more effective compared to the case of two positive charges. This result is understandable in that positive charges act as attractive sources, while negative charges produce a repulsive field and, consequently, do not present confined states near the impurity center. The oscillations of the energies are accompanied by weak (less than 1% in amplitude) oscillations of the ground state average radius (not shown). Now, all states present oscillations on the average radius, but the more important ones occur when the negative charges are in a symmetric position ($z_1 = z_2$).

The principal trends of previous results can be qualitatively understood using a perturbation approach, as follows. The various field induced crossings $E_0(B) = E_1(B)$ of an ideal QR involve two states, differing by one unit of angular momentum ($|\Delta l_z| = \hbar$). One can show on very general grounds, and for an arbitrary distribution of N impurities of charge Z_p located at $\vec{r}_p = (\vec{\rho}_p, z_p)$ ($p = 1, \ldots, N$), that the AB crossings should be replaced by anticrossings whenever the quantity $\Sigma_{p=1}^{N} Z_p \exp(-q_\perp |z - z_p|) \exp(i\theta_p) J_1(\rho_p q_\perp)$ does not vanish, where $J_1(x)$ is a Bessel function and $q_\perp$ a wave vector that results from a two-dimensional Fourier decomposition of the impurities potential. Indeed, this is the quantity that one gets, after integration over the in-plane angular variable, when evaluating the matrix element of the impurity potential between the two crossing states. This quantity (and thus the full matrix element) never vanishes in the single impurity case [provided it is not placed in the QR axis ($\rho_p = 0$)]. For two impurities with equal charge (same Z_p) and at the same in-

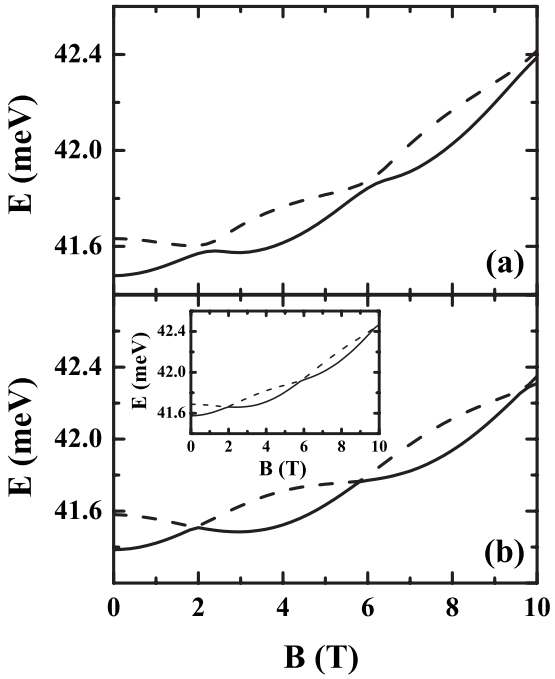

FIG. 6. Energy of the ground state (solid line) and first excited state (dashed line) with two negative hydrogenic impurities nearby a QR with size $a=140$ Å and $b=240$ Å with the first impurity at $\vec{r}_{imp}^{(1)}=(190\ \text{Å},0,z_1)$ and the second one at $\vec{r}_{imp}^{(2)}=(-190\ \text{Å},0,z_2)$. (a) $z_1=10$ Å and $z_2=30$ Å and (b) $z_1=z_2=30$ Å and $z_1=z_2=10$ Å in the inset, respectively.

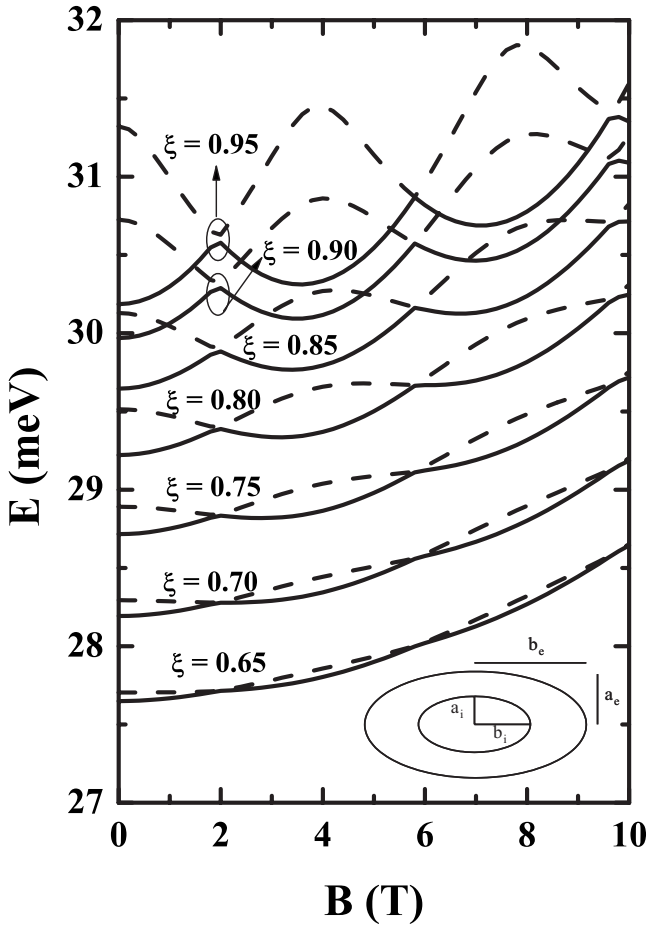

FIG. 7. Energy of the ground (solid line) and the first excited (dashed line) state as a function of the external magnetic field with different values of eccentricity, $R_I=140$ Å, and $R_E=240$ Å.

plane distance from the QR axis (same ρ_p), this term vanishes for $z_1=z_2$ and $\theta_2=\theta_1+\pi$. Note finally that we always have B-induced crossings for impurities located in the QR axis (as, e.g., discussed in Refs. 16 and 17).

IV. GEOMETRICAL EFFECTS ON ELECTRONIC LEVELS

To study geometrical effects on the AB oscillations, we consider elliptical QRs composed of concentric ellipses. To more clearly analyze the geometrical effects, we will consider systems which present different eccentricities, but with the same area in order to have an equal magnetic flux through the rings, without the presence of impurities. The internal ($j=I$) and external ($j=E$) interfaces of the ring are ellipses with eccentricities $\xi_j=a_j/b_j$, with minor (major) axis $a_j=R_j\sqrt{\xi_j}$ ($b_j=R_j/\sqrt{\xi_j}$) (see Fig. 7). Let us start with an elliptical ring with same internal and external eccentricities ξ and with $R_I=140$ Å and $R_E=240$ Å. Figures 7 and 8 present, respectively, the energies and the average radii of both the ground and first excited states as a function of the external magnetic field for different values of the eccentricity. We first observed that the AB oscillations are suppressed when ξ decreases. In fact, when ξ decreases the first two states tend to become degenerated and the densities of charge are localized in the regions of the QR of largest curvature. The decrease of the amplitude of the AB oscillations when ξ decreases is similar to the one obtained for two positive impurities (with $z_1=z_2$ and symmetric in-plane positions) when z_i decreases.

A criterion for the appearance of the spatial localization and the suppression of the AB oscillations can be obtained if we recall that the characteristic level spacing $E_1(0)-E_0(0)$ of a circular QR is roughly proportional to $1/R^2$, where R is the QR average radius. For the elliptical QRs in Figs. 7 and 8, one has $R=R(\theta)=b\cos^2(\theta)+a\sin^2(\theta)$. The suppression of the AB oscillation is expected to arise when the amplitude of the angular variation of the characteristic level spacing becomes comparable to its value for the mean QR [circular QR with average radius $R_{av}=(a+b)/2$], that is, when $1/R_{av}^2=1/a^2-1/b^2$. For the parameters in Figs. 7 and 8, this means eccentricities less than $\xi=0.6$, in very good agreement with the fully numerical results.

A different geometrical change in QR is to consider a system where the internal barrier has cylindrical symmetry and the external one is a concentric ellipse (system A). This system can be experimentally expected due to the mismatch of the lattice parameters in the formation of the QRs. Let us consider the case where the internal interface has a radius $R_I=140$ Å and the external ellipse presents an eccentricity ξ with minor (major) axis $a_j=R_E\sqrt{\xi}$ ($b_j=R_E/\sqrt{\xi}$) with $R_E=240$ Å. In Fig. 9, we present the energies of the ground and the first excited states as a function of the external magnetic field with different values of eccentricity and compared with

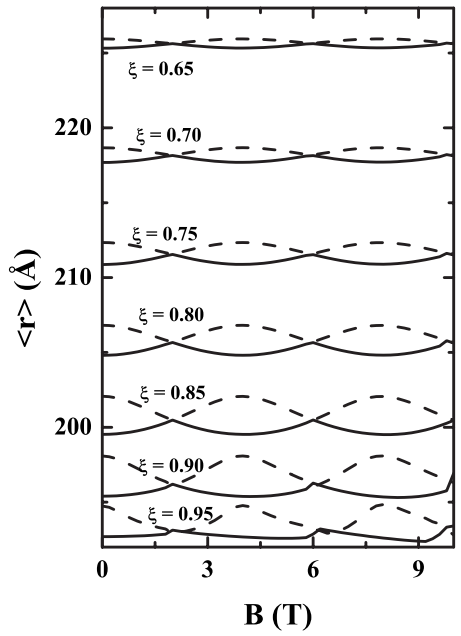

FIG. 8. Average radius of the ground state (solid line) and the first excited (dashed line) as a function of the external magnetic field with different values of eccentricity. Same QR parameters as in Fig. 7.

the energies of QRs composed by concentric ellipses of the same area (system B). For system B, we used the same definitions for the minor (major) axis of the concentric ellipses and considered for the internal (external) ellipse R_I=140 Å

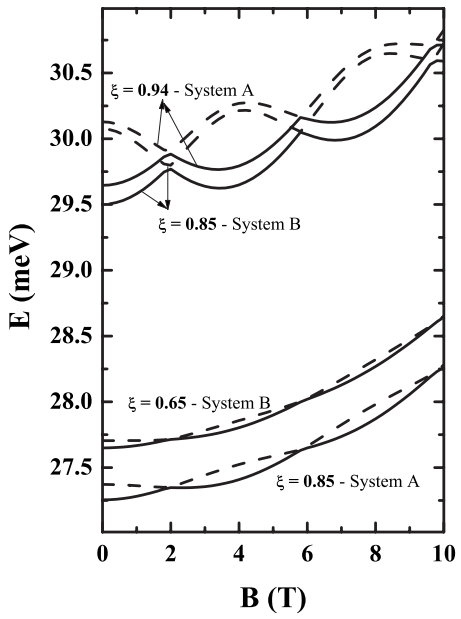

FIG. 9. Energy of the ground state (solid line) and the first excited state (dashed line) as a function of the external magnetic field with different values of eccentricity and for the case when the QR internal barrier has cylindrical symmetry and the external one is a concentric ellipse (system A), and when the QRs are composed by concentric ellipses (system B), having the same area.

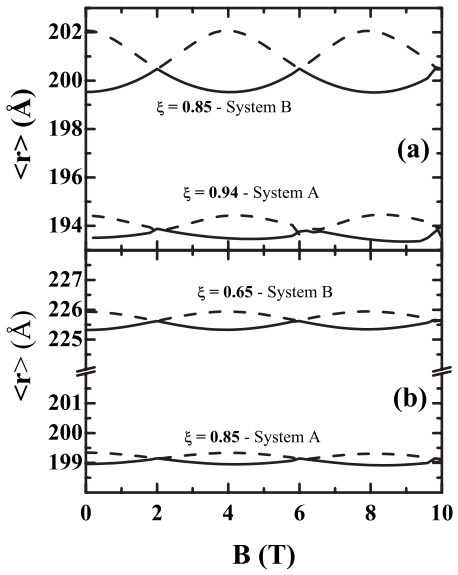

FIG. 10. Average radius of the ground state (solid line) and the first excited state (dashed line) as a function of the external magnetic field for the same systems as in Fig. 9.

(R_E=240 Å). Since both systems have the same area, the minima and maxima of the oscillations occur at the same values of the magnetic field. Also, oscillations of the same order of magnitude come out for very different values of the eccentricity: corresponding to ξ=0.94 and ξ=0.85 for system A and ξ=0.85 and ξ=0.65 for system B. This difference obtains because in system B the width of the ring is constant, while in system A, the ring width is very small along the minor axis, compared to its value along the major axis. Consequently, the wave function in system A will be localized in the regions close to the major ellipse axis, corresponding to two quasidegenerate states, similar to the effect of two positive impurities charges. The average radius of systems A and B are shown in Fig. 10. As expected, the systems that present small energy oscillations (A with ξ=0.85 and B with ξ=0.65) have low oscillations on the average radius [see Fig. 10(b)]. In the systems with energies of the same order of magnitude, the corresponding average radii in B are always bigger than the ones in system A since concentric ellipses (system B) have higher eccentricities compared to system A.

Another change in geometrical parameters in QRs is to consider the existence of roughness at the ring interfaces. These correspond to protrusions of barrier material in the ring region or vice-versa. Here, we simulate one QR with rough interfaces by assuming that the internal and external interface radii can be described by a function of the type (see, e.g., Ref. 25),

$$R(\theta) = R_{av} + r(\theta), \tag{4}$$

$$r(\theta) = 2\sigma_R \sqrt{\frac{L_C}{\sqrt{2\pi}R_{av}}} \sum_{n>0} \exp\left[-\left(\frac{nL_C}{2R_{av}}\right)^2\right] \cos(n\theta + \varphi_n), \tag{5}$$

where θ is the in-plane angle, φ_n are aleatory phases, R_{av} is the average radius, $(\langle r(0)^2\rangle)^{1/2}=\sigma_R$ the mean displacement

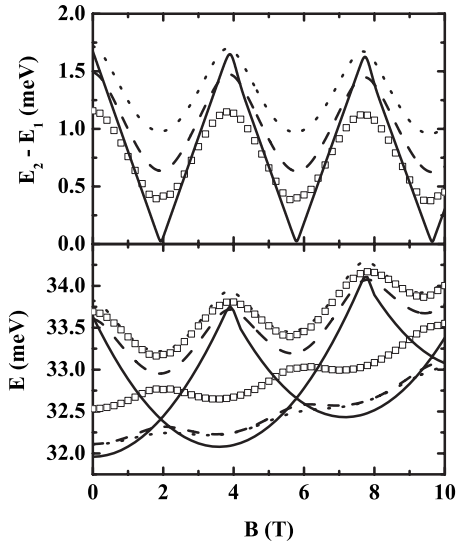

FIG. 11. Energies of the first two QR states (bottom) and their energy difference (top) as a function of the external magnetic field, considering an ideal QR (solid line) and a QR with roughness at the internal (dotted line) at the external (dashed line) and at both interfaces (square symbol).

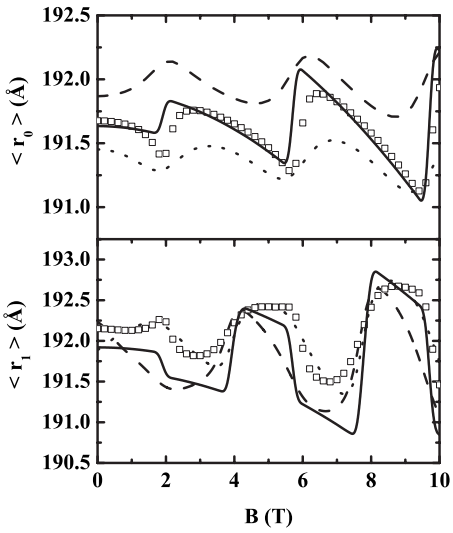

FIG. 12. Average radius of the ground state ($\langle r_0 \rangle$) and first excited state ($\langle r_1 \rangle$) as a function of the external magnetic field considering an ideal QR (solid line) and a QR with roughness at the internal (dotted line) at the external (dashed line) and at both interfaces (square symbol).

from the average radius, and L_C is the correlation length of the interface radius. The three parameters (set of φ_n, L_C, and σ_R) are in general different for the inner ($R_{av}=R_I$) and outer ($R_{av}=R_E$) interfaces.

To analyze the effects of roughness, we present in Fig. 11 the energies of the ground and first excited states as a function of the external magnetic field, considering an ideal QR (circular interfaces) and for rings with roughness at only the internal, only the external, or at both interfaces (R_I=140 Å, R_E=240 Å, $\sigma_{RI}=\sigma_{RE}$=5 Å, and $L_{CRI}=L_{CRE}$=10 Å). The AB oscillations are present in all cases. However, the disorder in any case transforms the field-induced AB crossing of the ideal QR into anticrossings. This is because the disorder potential has a nondefined angular dependence with, in particular, a nonvanishing $|\Delta l_z|=\hbar$ component, which is able to couple the two crossing states of the ideal QR. Note that this is never the case for the different eccentricity configurations discussed above, which all have a D-like in-plane symmetry and thus are unable to lift the field-induced AB crossing between the first two QR states. In Fig. 12, we show the average radius of the ground and first excited states as a function of the external magnetic field associated with the states presented in Fig. 11. With the QR with ideal interfaces, there is an abrupt change in some values of the magnetic field, but depending on what interface roughness is present, a smooth transition is observed between the ground and first excited state for the same values of the magnetic field.

V. CONCLUSION

In this work, we have calculated the electronic states of a semiconductor quantum ring in the presence of an axial uniform magnetic field. We have considered the effect of different static perturbations on the energy spectrum of the QR and considered, in particular, the effect of the disorder upon its AB oscillations. To this aim, and contrary to previous theoretical works, we have applied a nonperturbative method, which can be used for disorder of any strength. This has the advantage of simultaneously enabling us to tackle important defect perturbations, like the ones due to the presence of charged impurity centers nearby the QR, while allowing not only the description of the electron ground state but also of the excited QR states. Our results show that the AB oscillations are very sensitive to the nature of the disorder. For instance, an eccentricity in the ring geometry never washes out the leading AB oscillations (and the field-induced crossings) but may considerably decrease their amplitude: this is because an important eccentricity generates a preferential localization of the electron wave functions near the regions of largest curvature. On the contrary, random roughness in the QR interfaces always lifts the field-induced crossings that occur in a perfect QR but affects to a lesser extent the oscillations amplitude (since in the general case, it does not lead to any preferential localization along the QR circumference). Finally, impurity centers, which are expected to be present in actual structures, may considerably affect the energy spectrum. For instance, a charged center placed nearby the QR region will suppress the oscillations of the energies with the applied field.

ACKNOWLEDGMENTS

G.A.F., M.H.D., and J.A.K.F. are supported the Brazilian National Research Council (CNPq) under contract Nano-BioEstruturas 555183/2005-0, Fundação Cearense de Apoio ao Desenvolvimento Científico e Tecnológico (Funcap). These authors and R.F. benefit from a CAPES/COFECUB contract (457/04). The Laboratoire Pierre Aigrain is "Unité

mixte de Recherche (UMR 8551) du C.N.R.S., Université Paris VI et Université Paris VII."

APPENDIX

In the numerical calculations, we consider our system placed inside a large square hard box of side L. In the presence of an external magnetic field, we replace $\vec{p}$ by $\vec{p}+e\vec{A}$ and use the expansion proposed by Suzuki.[26] The time evolution of the wave function [Eq. (3)] can be written as

$$\Psi(\vec{r},t+\Delta t)=\exp\left[\frac{-i\Delta t}{2\hbar}V(\vec{r})\right]\exp\left(\frac{-i\Delta t}{\hbar}T\right)\exp\left[\frac{-i\Delta t}{2\hbar}V(\vec{r})\right]\times\Psi(\vec{r},t)+O(\Delta t^3), \tag{A1}$$

where the total kinetic energy is $T=T_x+T_y$, where

$$T_x=\frac{1}{2m^*}(p_x-eyB/2)^2=\frac{1}{2m^*}\left[-i\hbar\frac{\partial}{\partial x}-eyB/2\right]^2,$$

$$T_y=\frac{1}{2m^*}(p_y+exB/2)^2=\frac{1}{2m^*}\left[-i\hbar\frac{\partial}{\partial y}+exB/2\right]^2. \tag{A2}$$

The error introduced in this expansion by dropping the term $O(\Delta t^3)$ results from the fact that kinetic and potential operators do not commute. Note that, at first glance, we could be tempted to use cylindrical coordinates since we are dealing with electrons in a quantum ring. However, our final purpose is to analyze the effects of impurities and geometrical defects in these systems, which break the cylindrical ring geometry. For this reason, it is more convenient to use Cartesian coordinates (which are also easier to numerically implement) in our numerical calculations.

At nonzero magnetic field, T_x and T_y do not commute and

$$\exp\left[\frac{-i\Delta t}{\hbar}(T_x+T_y)\right]=\exp\left[\frac{-i\Delta t}{\hbar}T_y\right]\exp\left[\frac{-i\Delta t}{\hbar}T_x\right]+O[B(\Delta t^2)]. \tag{A3}$$

To proceed further within this approximation, we define

$$\eta(\vec{r},t+\Delta t)=\exp\left[\frac{-i\Delta t}{\hbar}T_y\right]\eta'(\vec{r},t+\Delta t), \tag{A4}$$

$$\eta'(\vec{r},t+\Delta t)=\exp\left[\frac{-i\Delta t}{\hbar}T_x\right]\xi(\vec{r},t+\Delta t), \tag{A5}$$

and

$$\xi(\vec{r},t+\Delta t)=\exp\left[\frac{-i\Delta t}{2\hbar}V(\vec{r})\right]\Psi(\vec{r},t), \tag{A6}$$

When we study systems with periodic boundary conditions, the exponential containing the kinetic operator is efficiently treated by the fast Fourier transform since it is diagonal in reciprocal space. However, when the system is not periodic, we use the following expansion (see, e.g., Ref. 27):

$$\exp\left[\frac{-i\Delta t}{\hbar}T_x\right]\cong\left[1+\frac{i\Delta t}{2\hbar}T_x\right]^{-1}\left[1-\frac{i\Delta t}{2\hbar}T_x\right]+O(\Delta t^3). \tag{A7}$$

Equation (A5) can thus be written as

$$\left\{1+i\hbar\frac{\Delta t}{4m^*}\left[-\frac{\partial^2}{\partial x^2}-\frac{eyB}{i\hbar}\frac{\partial}{\partial x}+\left(\frac{eyB}{2\hbar}\right)^2\right]\right\}\eta'(\vec{r},t+\Delta t)=\left\{1-i\hbar\frac{\Delta t}{4m^*}\left[-\frac{\partial^2}{\partial x^2}-\frac{eyB}{i\hbar}\frac{\partial}{\partial x}+\left(\frac{eyB}{2\hbar}\right)^2\right]\right\}\xi(\vec{r},t+\Delta t). \tag{A8}$$

Using the finite difference method to discretize the functions $\eta'(\vec{r},t+\Delta t)$, $\xi(\vec{r},t+\Delta t)$, and their derivatives, Eq. (A8) can be written for numerical purposes as

$$-\beta_x(1+i\alpha^y)\eta'_{i-1}+\{1+\beta_x[2+(\alpha^y)^2]\}\eta'_i-\beta_x(1-i\alpha^y)\eta'_{i+1}=\beta_x(1+i\alpha^y)\xi_{i-1}+\{1-\beta_x[2+(\alpha^y)^2]\}\xi_i+\beta_x(1-i\alpha^y)\xi_{i+1}, \tag{A9}$$

where $\alpha^y=\Delta x\omega_c\hbar y/4R_y$ and $\beta_x=iR_y\Delta t/2\hbar(\Delta x)^2$, being ω_c and R_y the effective cyclotron resonance and Rydberg, respectively, and Δx and Δy the mesh in real space.

Using the same procedure for the propagation related to the T_y operator, we obtain for Eq. (A4),

$$-\beta_y(1+i\alpha^x)\eta_{i-1}+\{1+\beta_y[2+(\alpha^x)^2]\}\eta_i-\beta_y(1-i\alpha^x)\eta_{i+1}=\beta_y(1+i\alpha^x)\eta'_{i-1}+\{1-\beta_y[2+(\alpha^x)^2]\}\eta'_i+\beta_y(1-i\alpha^x)\eta'_{i+1}, \tag{A10}$$

with $\alpha^x=-\Delta y\omega_c\hbar x/4R_y$ and $\beta_y=iR_y\Delta t/2\hbar(\Delta y)^2$. In Eqs. (A9) and (A10), the variables x, y, Δx, and Δy are in units of effective Bohr radius.

With Eqs. (A9) and (A10), the wave function propagation is now reduced to a matrix problem. For a time-independent Hamiltonian, the propagation is time-reversal invariant and conserves the total energy. In order to obtain the electron eigenstates, the outline described above is applied to an initial Gaussian wave packet and the evolution is made in the imaginary time domain, that is, one substitutes t by $-i\tau$. After a few steps, the wave function converges to the ground state of the system. The excited states are obtained using the same procedure, in combination with a Gram-Schmidt orthonormalization. Typically, to obtain numerical convergence, we use a mesh of $N_x=N_y=141$ squares with sides of 5 Å each, $\Delta t=0.2$ fs, and we propagate the wave function up to $N_t=28\times10^3$ time steps.

*gil@fisica.ufc.br
†degani@fisica.ufc.br
‡king@fisica.ufc.br
§jusciane@fisica.ufc.br
‖robson.ferreira@lpa.ens.fr

[1] B. Szafran and F. M. Peeters, Europhys. Lett. **12**, 271 (2005).
[2] H. W. Choi, C. W. Jeon, C. Liu, I. M. Watson, M. D. Dawson, P. R. Edwards, R. W. Martin, S. Tripathy, and S. J. Chua, Appl. Phys. Lett. **86**, 021101 (2005).
[3] T. Kuroda, T. Mano, T. Ochiai, S. Sanguinetti, K. Sakoda, G. Kido, and N. Koguchi, Phys. Rev. B **72**, 205301 (2005), and references therein.
[4] Boris S. Monozon, Mikhail V. Ivanov, and Peter Schmelcher, Phys. Rev. B **70**, 205336 (2004).
[5] L. G. G. V. Dias da Silva, S. E. Ulloa, and A. O. Govorov, Phys. Rev. B **70**, 155318 (2004).
[6] B. S. Monozon and P. Schmelcher, Phys. Rev. B **67**, 045203 (2003).
[7] T. Raz, D. Ritter, and G. Bahir, Appl. Phys. Lett. **82**, 1706 (2003).
[8] Daniel Granados and Jorge M. Garcia, Appl. Phys. Lett. **82**, 2401 (2003).
[9] Z. Barticevic, M. Pacheco, and A. Latgé, Phys. Rev. B **62**, 6963 (2000).
[10] A. Lorke, R. J. Luyken, A. O. Govorov, J. P. Kotthaus, J. M. Garcia, and P. M. Petroff, Phys. Rev. Lett. **84**, 2223 (2000).
[11] Y. Aharonov and D. Bohm, Phys. Rev. **115**, 485 (1959).
[12] A. Bruno-Alfonso and A. Latgé, Phys. Rev. B **61**, 15887 (2000).
[13] Jakyoung Song and Sergio E. Ulloa, Phys. Rev. B **63**, 125302 (2001).
[14] Hui Hu, Jia-Lin Zhu, Dai-Jun Li, and Jia-Jiong Xiong, Phys. Rev. B **63**, 195307 (2001).
[15] A. Bruno-Alfonso and A. Latgé, Phys. Rev. B **71**, 125312 (2005).
[16] C. M. Lee, W. Y. Ruan, J. Q. Li, and Ricard C. H. Lee, Phys. Rev. B **71**, 195305 (2005).
[17] C. M. Lee, J. Q. Li, W. Y. Ruan, and Ricard C. H. Lee, Phys. Rev. B **73**, 212407 (2006).
[18] L. G. G. V. Dias da Silva, S. E. Ulloa, and T. V. Shahbazyan, Phys. Rev. B **72**, 125327 (2005).
[19] M. Aichinger, S. A. Chin, E. Krotscheck, and E. Räsänen, Phys. Rev. B **73**, 195310 (2006).
[20] L. A. Lavenère-Wanderley, A. Bruno-Alfonso, and A. Latgé, J. Phys.: Condens. Matter **14**, 259 (2002).
[21] D. Gridin, A. T. I. Adamou, and R. V. Craster, Phys. Rev. B **69**, 155317 (2004).
[22] M. H. Degani, Appl. Phys. Lett. **59**, 57 (1991).
[23] M. H. Degani and J. P. Leburton, Phys. Rev. B **44**, 10901 (1991).
[24] M. H. Degani, Phys. Rev. B **66**, 233306 (2002).
[25] J. M. Ziman, *Models of Disorder* (Cambridge University Press, Cambridge, 1979).
[26] M. Suzuki, Phys. Lett. A **146**, 319 (1990).
[27] W. H. Press, B. P. Flannery, S. A. Teukolsky, and W. T. Vetterling, *Numerical Recipes: The Art of Scientific Computing* (Cambridge University Press, Cambridge, 1989), p. 642.